Organic & Biomolecular Chemistry

PAPER

View Article Online
View Journal | View Issue

Cite this: *Org. Biomol. Chem.*, 2018, **16**, 609

Design of a substrate-tailored peptiligase variant for the efficient synthesis of thymosin-α_1†

Marcel Schmidt,[a,b] Ana Toplak,[a] Henriëtte J. Rozeboom,[c] Hein J. Wijma,[c] Peter J. L. M. Quaedflieg,[a] Jan H. van Maarseveen,[b] Dick B. Janssen[c] and Timo Nuijens*[a]

The synthesis of thymosin-α_1, an acetylated 28 amino acid long therapeutic peptide, *via* conventional chemical methods is exceptionally challenging. The enzymatic coupling of unprotected peptide segments in water offers great potential for a more efficient synthesis of peptides that are difficult to synthesize. Based on the design of a highly engineered peptide ligase, we developed a fully convergent chemo-enzymatic peptide synthesis (CEPS) process for the production of thymosin-α_1 *via* a 14-mer + 14-mer segment condensation strategy. Using structure-inspired enzyme engineering, the thiol-subtilisin variant peptiligase was tailored to recognize the respective 14-mer thymosin-α_1 segments in order to create a clearly improved biocatalyst, termed thymoligase. Thymoligase catalyzes peptide bond formation between both segments with a very high efficiency (>94% yield) and is expected to be well applicable to many other ligations in which residues with similar characteristics (*e.g.* Arg and Glu) are present in the respective positions P1 and P1′. The crystal structure of thymoligase was determined and shown to be in good agreement with the model used for the engineering studies. The combination of the solid phase peptide synthesis (SPPS) of the 14-mer segments and their thymoligase-catalyzed ligation on a gram scale resulted in a significantly increased, two-fold higher overall yield (55%) of thymosin-α_1 compared to those typical of existing industrial processes.

Received 16th November 2017,
Accepted 21st December 2017

DOI: 10.1039/c7ob02812a

rsc.li/obc

Introduction

Owing to their outstanding biological selectivity and efficacy, exploiting peptides as therapeutics has become increasingly popular. Their therapeutic potential addresses the full scope of medical disorders with currently over 60 peptides approved in major markets and over 150 peptides in active development today.[1,2] The peptide therapeutics market is expected to reach about $25 billion by 2020[3] and its growth is accompanied by an increased demand for new and more efficient processes for their production on the industrial scale. The manufacture of long peptides using conventional chemical strategies is still very challenging and the technology used has remained almost unchanged since Merrifield developed the solid phase approach in the 1960s.[4] Solid-phase peptide synthesis (SPPS) is characterized by an exponential decrease in the crude yield and purity as the peptide length increases: coupling and deprotection steps become less efficient and purification from accumulating by-products becomes increasingly difficult. In contrast, segment condensation processes are intrinsically more efficient, since short peptide segments can be produced in high yield and purity. However, the chemical ligation of peptide segments is still a significant challenge, mainly due to the low solubility of the protected segments and the potential epimerization of the C-terminal amino acid upon activation. To overcome some of these difficulties, the application of chemo-enzymatic peptide synthesis (CEPS), a combination of conventional SPPS for the production of unprotected peptide segments and an enzymatic epimerization-free coupling of the segments in water, represents a promising strategy. Hence, enzyme-mediated ligation technologies, *e.g.* the use of sortases,[5] butelase-1,[6,7] trypsiligase[8,9] and subtilisin variants such as subtiligase[10,11] or peptiligases,[12,13] have recently gained increased attention for a more cost-efficient synthesis of medium-sized or long peptides.[14]

A well-known peptide that is difficult to synthesize using conventional methodologies is thymosin-α_1, an acetylated 28-mer therapeutic peptide (Ac-SDAAVDTSSEITTKDLKEKKEVVEEAEN-OH, 3108.32 g mol^{-1}) with immunoregulating activity.

[a]*EnzyPep B.V., Brightlands Campus, Urmonderbaan 22, 6167 RD Geleen, The Netherlands. E-mail: timo@enzypep.com; Tel: +31-464760675*
[b]*Van 't Hoff Institute of Molecular Sciences, University of Amsterdam, Science Park 904, 1098 XH Amsterdam, The Netherlands*
[c]*Groningen Biomolecular Science and Biotechnology Institute, University of Groningen, Nijenborgh 4, 9747 AG Groningen, The Netherlands*

† Electronic supplementary information (ESI) available: Experimental details and supplementary results. See DOI: 10.1039/c7ob02812a

After administration, thymosin-α_1 elicits a variety of immune system responses and is being used for a range of medical applications (*e.g.* treatment of hepatitis B and C).[15–17] It is approved in more than 30 countries and mainly marketed in China.[17] Triggered by the market demand, several solid- and solution phase strategies have been developed during the past few decades. However, these repeatedly resulted in low overall yields (approx. 25%).[18–25] The synthesis of thymosin-α_1 is especially hampered by the large number of protecting groups required (20 in total) and its tendency to form β-sheets.[26] Approaches for the production of the highly acidic peptide in pro- or eukaryotic expression systems as a cost-effective alternative resulted in low titers (<30 mg L^{-1} of cell culture)[27,28] and even more difficult isolation and purification procedures compared to full SPPS.

The feasibility of a chemo-enzymatic approach is critically dependent on the availability of an enzyme capable of efficiently forming a peptide bond between two peptide segments. A successful example of a kinetically controlled peptide ligation strategy is the use of a highly engineered, stabilized and Ca^{2+}-independent thiol-subtilisin variant termed peptiligase.[12,13] Using peptiligase, a peptide segment that is C-terminally activated as a carboxamidomethyl(Cam)-ester (acyl donor) can be coupled with a peptide segment with a free nucleophilic N-terminus (acyl acceptor) in high yield. However, when engineered proteases such as peptiligase were used, hydrolytic side-reactions may occur, including the hydrolysis of the acyl donor ester moiety and a very slow hydrolysis of the final product. Hence, the minimization of these side-reactions is required in order to maximize the product yield.

Earlier engineering studies already indicated that peptiligase can serve as a template for engineering variants with dedicated selectivity and improved performance.[13] When we tested the use of peptiligase for a [14 + 14]-mer coupling strategy to synthesize thymosin-α_1 (Fig. 1A), a low coupling yield (<20%) and significant hydrolysis of the acyl donor ester was observed (Fig. 4). Thus, in order to obtain a dedicated biocatalyst for this purpose, we followed a structure-based enzyme design approach. Ultimately, enzyme engineering yielded the improved peptiligase variant, thymoligase, that allowed the efficient synthesis of thymosin-α_1 using a [14 + 14]-mer segment condensation approach.

Results and discussion

Substrate-tailored, structure-inspired enzyme engineering

To explore the chemo-enzymatic synthesis of thymosin-α_1, we initially tested peptiligase in a [14 + 14]-mer segment coupling under conditions similar to those reported for the synthesis of the incretin mimetic drug exenatide.[13] These initial experiments resulted in the formation of thymosin-α_1 with a very low efficiency, with a yield (the acyl donor substrate converted to the synthetic product) below 20% (Fig. 4). In addition, the S/H ratio (the ratio between the desired synthetic product and the hydrolyzed acyl donor) was also very low. In earlier mutagenesis studies, substitution M222G was introduced to reduce sensitivity towards oxidation[29] and to reduce steric crowding in the active site of peptiligase[13] with the aim of improving the coupling efficiency. Indeed, the introduction of this mutation (giving the variant Ptl G) improved the synthetic yield to 33% (Fig. 2A), which was, however, still unsatisfactory.

To discover mutations that would drastically improve the performance in the synthesis of thymosin-α_1, we examined structural models of peptiligase. For this, we constructed a hybrid model using YASARA with pdb files 1GNV[30] (calcium-independent subtilisin BPN′) and 1SBN[31] (subtilisin–eglin complex). A segment of thymosin-α_1 [7–19] was modelled into the substrate binding region and the effects of additional mutations were examined using YASARA.[13] Based on this model, we identified residues that are in close contact with the substrate and aimed to introduce stabilizing interactions between the substrate and the respective binding pockets of peptiligase.

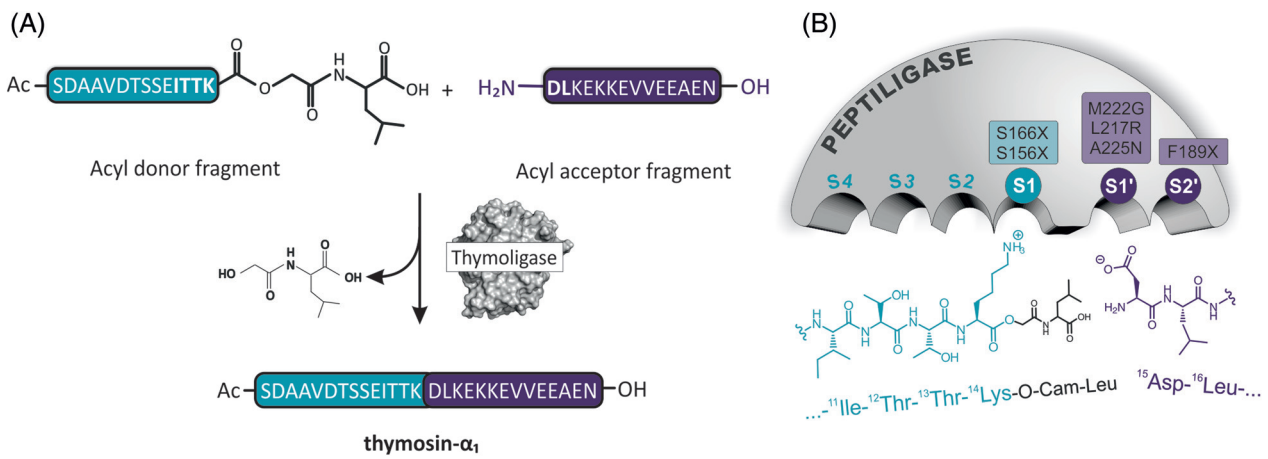

Fig. 1 (A) Overview of the thymosin-α_1 [14 + 14]-mer chemo-enzymatic coupling strategy and (B) schematic representation of the enzyme pockets of peptiligase with the particular positions, that were taken into account for the substrate-tailored enzyme engineering approach.

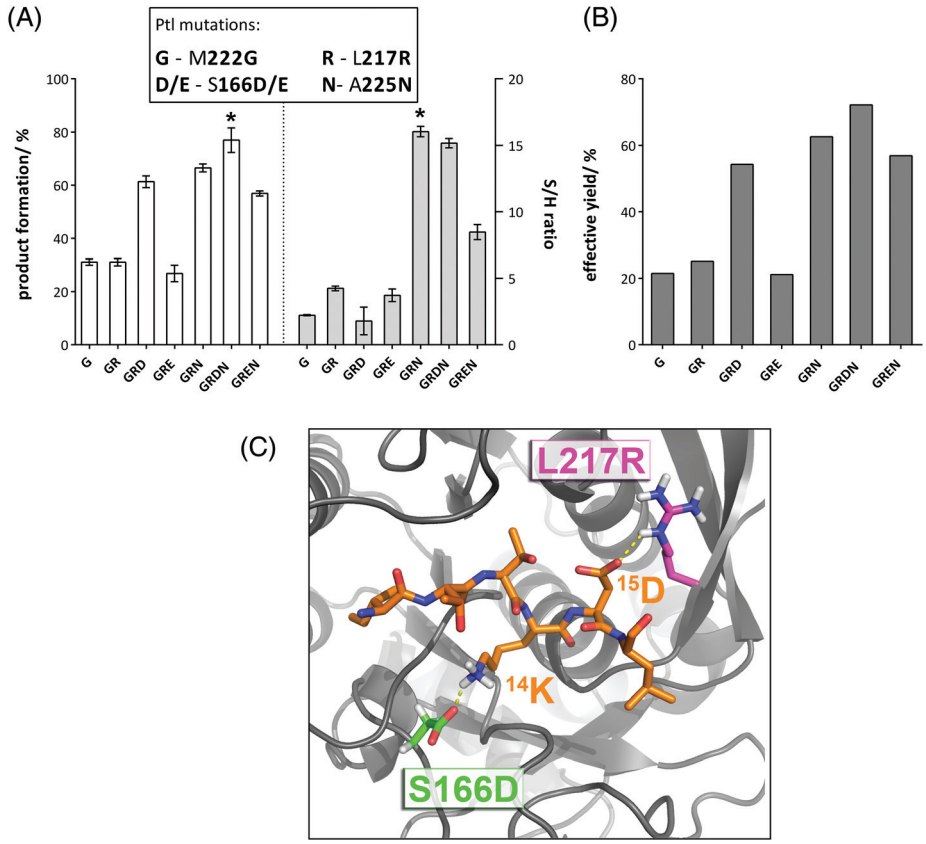

Fig. 2 (A) Result of testing of peptiligase variants for the thymosin-α_1 [14 + 14]-mer coupling efficiency. Variants bear different combinations of mutations M222G, L217R, S166D/E and A225N. Product formation (%) and S/H ratios after 60 min are shown. Couplings were performed in aqueous solution (1 M phosphate, pH 8.3, 3.5 mM TCEP, room temperature) using 0.7 μM of enzyme, crude Ac-Thm(1–14)-OCam-Leu-OH (14.3 mM) and crude H-Thm(15–28)-OH (17.1 mM). Errors are depicted as the SEM and the arithmetic mean is shown. The best performing variant is marked with a star (*). (B) Effective yields after 60 min are shown. The effective yield represents as a virtual measure of coupling efficiency. Effective yields are calculated by multiplying the amount of product formation after 60 min (%) with the S/H ratio (%) (*e.g.* an S/H ratio of 11.5 equals 92%). (C) Homology model of thymoligase GRDN. The enzyme backbone is shown in grey, crucial residues of the S1 pocket are shown in green and those of the S1′ pocket in magenta. Enzyme-bound partial thymosin-α_1 (ITTKDL) is indicated in orange and hydrogen bonds between the substrate and the enzyme are given in yellow. Nitrogen atoms are colored in blue, oxygen in red and hydrogens in grey/white.

For an efficient thymosin-α_1 [14 + 14]-mer coupling reaction, the enzyme is required to accept the positively charged ^{14}Lys side chain of the acyl donor in the S1 pocket as well as the negatively charged ^{15}Asp side chain of the acyl acceptor in the S1′ pocket (Fig. 1B). However, the inspection of the structural model of peptiligase suggested this to be problematic, especially as the S1 pocket is characterized by its hydrophobic nature that will not readily accept polar amino acids. Similarly, the ^{15}Asp of the nucleophilic segment will poorly fit in the S1′ pocket. Thus, our main design efforts focussed on tailoring the S1 and S1′ pockets for the acceptance of charged residues and, in addition, on fine tuning the enzyme by engineering the S2′ pocket to bind ^{16}Leu (Fig. 1B). The major residues shaping the S1 pocket are S156 and S166, therefore suggesting these to be targeted for mutagenesis. Similarly, L217 is prominent in the S1′ pocket. Mutations to consider include the introduction of a negatively charged residue at position S166 (S166D or S166E)[32] and a positively charged residue at position L217 (L217R).[13] Both could lead to the formation of ion pairs between the substrate and the enzyme (^{14}Lys/S166D and ^{15}Asp/L217R, Fig. 2C). In addition, polar amino acids in position S156 could also provide ionic interactions with the ^{14}Lys side chain of the substrate.

Enzyme variants were obtained using site-directed mutagenesis followed by heterologous expression in *B. subtilis* and subsequent His-tag purification (>80% SDS-PAGE purity, see ESI Fig. S4–S6†). The enzyme variants were screened for the [14 + 14] thymosin-α_1 coupling efficiency using crude 14-mer substrates, with only 1.2 eq. of the acyl acceptor segment being used.

Earlier studies on engineering the S1′ pocket revealed that mutation L217R enhances the coupling efficiency of small model peptides bearing an aspartic- or glutamic acid in position P1′.[13] In fact, we found that the introduction of mutation L217R into the Ptl M222G mutant (giving Ptl GR) resulted in a 2-fold increased S/H ratio in the [14 + 14] thymosin-α_1 coupling, while retaining the activity observed with Ptl G (Fig. 2A). Further combining mutations M222G and L217R with a nega-

tively charged amino acid residue in the S1 pocket (S166D) resulted in an even more active variant with double the product formation rate (Ptl GRD). However, although for this variant the S/H ratio is not improved compared to peptiligase M222G (Fig. 2A), the combined effects of the retained S/H ratio and improved product formation result in a significantly increased effective yield (Fig. 2B). In contrast, mutation S166E (Ptl GRE) resulted in an increased S/H ratio, but no improvement in activity and no increased effective yield was observed (Fig. 2A and B).

With a variant in hand that shows clearly the improved performance (Ptl GRD), we focused on further improving the S/H ratio. To this end, we addressed mutations at position A225, which is close to the S1′ pocket. Substitutions at this position can have positive effects, as was observed during the engineering of other peptiligase variants, such as omniligase-1.[33,34] Especially substitution A225N was shown to drastically improve the S/H ratio of different ligases in coupling reactions with short model peptides (unpublished results) and was therefore incorporated into the Ptl GR, GRD and GRE scaffolds. Indeed, the addition of mutation A225N increased both the activity and the S/H ratio of all variants, therefore resulting in an improved effective yield of the coupling (Fig. 2B). In particular, Ptl GRDN (M222G L217R S166D A225N) exhibited an exceptionally high coupling efficiency (77%) and a more than seven-fold increase of the S/H ratio compared to Ptl GRD (Fig. 2A). The homology model of Ptl GRDN revealed two hydrogen bonds between S166D/^{14}K and L217R/^{15}D, which could potentially lead to an improved overall performance of this variant (Fig. 2C). Peptiligase M222G L217R A225N, which does not have an additional negative charge in the S1 pocket, also performed extraordinarily well, with conversions similar to Ptl GRDN and an even slightly higher S/H ratio. However, the higher overall performance of Ptl GRDN emphasizes again the importance of mutation S166D for an efficient ligation (Fig. 3C). The best enzyme from the stepwise rational engineering approach, *i.e.* Ptl GRDN, was chosen as the starting point for further optimization of the S1 pocket. Ptl GRDN carries a negative charge at the bottom of the S1 pocket (due to S166D) and we examined the effect of substitutions at position S156, located in proximity to position S166. Wells *et al.* showed that subtilisin BPN′ carrying negatively charged residues at positions S156 and S166 is able to form ion pairs with positively charged acyl donors and the effects on binding appeared to be additive.[32] For example, a net charge of −2 (S166D; S156E/D) could possibly improve the binding of positively charged amino acids in the S1 pocket. Moreover, the additional negative charge could electrostatically affect the adjacent N155, which plays a key role in transition state stabilization.[35] Hence, the effect of the introduction of a second ion pair (*i.e.* S156D/E) at the S1 subsite was investigated (Fig. 3A). Consequently, serine at position 156 was mutated to different polar and charged amino acids (S156X – X: E, Q, D, N, T). Non-polar amino acids served as a negative control (S156X – X: A, L). In contrast to a negative charge being generally beneficial in position 166, the effects of an additional negative charge at position 156 appear to vary. A three-fold decrease in product formation with an unaltered

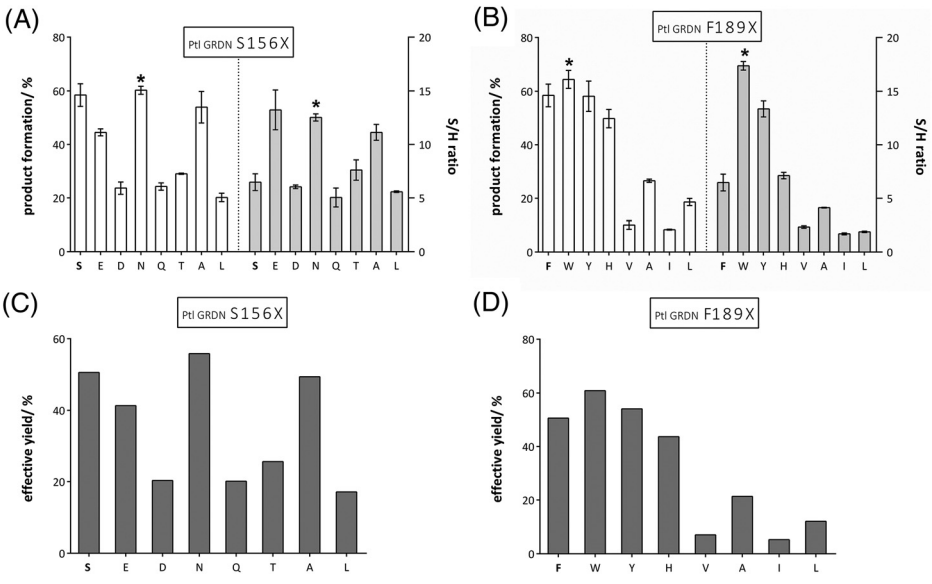

Fig. 3 Result of testing the peptiligase variants library GRDN (M222G, L217R, S166D, A225N) S156X (A) and F189X (B) for the thymosin-α_1 [14 + 14]-mer coupling efficiency. Product formation (%) and S/H ratios after 60 min are shown. Coupling reactions were performed in aqueous solution (1 M phosphate, pH 8.0, 3.5 mM TCEP, room temperature) using 0.35 μM of enzyme, crude Ac-Thm(1–14)-OCam-Leu-OH (7.15 mM) and crude H-Thm (15–28)-OH (8.55 mM). A slightly lower screening pH (8.0 *vs.* 8.3) was chosen compared to the conditions shown in Fig. 2A. In addition, the concentration of enzymes and substrates were halved compared to the conditions shown in Fig. 2. These sub-optimal conditions were used to clearly visualize the activity and efficiency differences of the peptiligase variants. Errors are depicted as the SEM and the arithmetic mean is shown. The best hit is marked with a star (*). (C) and (D) Effective yields after 60 min are shown. The effective yield represents a virtual measure of coupling efficiency. Effective yields are calculated by multiplying the amount of product formation after 60 min (%) with the S/H ratio (%).

S/H ratio was observed for the variant with two aspartic acid residues in the S1 pocket (S166D, S156D). On the other hand, the combination of S166D and S156E is well tolerated. Only a small reduction in product formation is observed and the S/H ratio actually doubled compared to the starting variant Ptl GRDN; however, not resulting in an increased effective yield (Fig. 3C). The best mutation introducing a polar group at position 156 was S156N (Fig. 3A). Despite the lack of a second charge in the S1 pocket, Ptl GRDN S156N fully retains its activity while clearly improving the S/H ratio almost three-fold. As expected, creating a smaller and more hydrophobic pocket by incorporating S156L resulted in a reduced overall performance compared to the starting variant (Fig. 3A and C). The same effect was observed when a branched polar residue was introduced at position S156 (S156T). This suggests that small polar, non-charged side chains at position 156 are a prerequisite for a high catalytic efficiency. Charges are tolerated, but not generally beneficial. Surprisingly, creating a larger S1 pocket (S156A) resulted in a higher S/H ratio and retained activity compared to the peptiligase variant bearing serine in position 156. Therefore, an ionic interaction of the substrate with the amino acid at position 156 seems to be beneficial, but not essential for retaining enzyme activity and obtaining high S/H ratios in the [14 + 14] thymosin-α_1 coupling.

In addition to engineering the S1 and S1′ pockets, an attempt was made to further improve the S/H ratio by varying the position F189, located in the hydrophobic S2′ pocket. In the case of the thymosin-α_1 [14 + 14] coupling strategy, hydrophobic ^{16}Leu is present at position P2′. Hence, we examined the substitutions with other apolar amino acids (F189X – X: W, Y, H, V, A, I, L) that may increase the hydrophobic interactions between the enzyme and the substrate. The results clearly indicated that aromatic amino acids in position 189 exhibit a positive overall effect resulting in a remarkably increased S/H ratio, whereas small hydrophobic amino acids (V, A, I, L) led to less than 50% product formation (Fig. 3B) and in general a considerably reduced overall performance (Fig. 3D) compared to Ptl GRDN. The aromatic rings form a more defined, rigid hydrophobic surface in the S2′ pocket and could play a role in π-stacking stabilizing interactions. Beside the hydrophobic nature of their side chains, the residues that are also hydrogen bond donors exhibit a higher overall performance (W > Y > H > F, Fig. 3B). Ptl GRDN F189W (Ptl GRDNW) shows the highest product formation rate and S/H ratio, resulting in a high effective yield of the ligation (Fig. 3D).

Finally, we tested whether mutations S156N and F189W had an additive effect if combined into the Ptl GRDN backbone. Indeed, Ptl GRDN F189W S156N, termed thymoligase, noticeably outperformed the best variant so far, *i.e.* Ptl GRDNW. A 10% higher coupling yield and a 35% higher S/H ratio was achieved (Fig. 4). The comparison of peptiligase variants from different stages unequivocally demonstrates the successful design of this powerful ligase, enabling an efficient [14 + 14]-mer thymosin-α_1 segment condensation. Thymoligase features a more than 5-fold higher reaction yield and a more than 20-fold increased preference for peptide bond formation over hydrolysis compared to peptiligase (see Fig. 4). The effective yield of the ligation could be increased more than 10-fold (Fig. 4B). In particular, designing the S1 (S166D and S156N) and S1′ (L217R) pockets by introducing electrostatic interactions with the substrate P1 and P1′ positions resulted in the successful tailoring of thymoligase towards charged substrates. F189W and A225N also represent key mutations, which resulted in an improved product formation and a significant increase of the S/H ratio (see Fig. 4).

X-ray crystal structure determination

In order to verify the accuracy of the models used, the three-dimensional structure of thymoligase was determined by X-ray

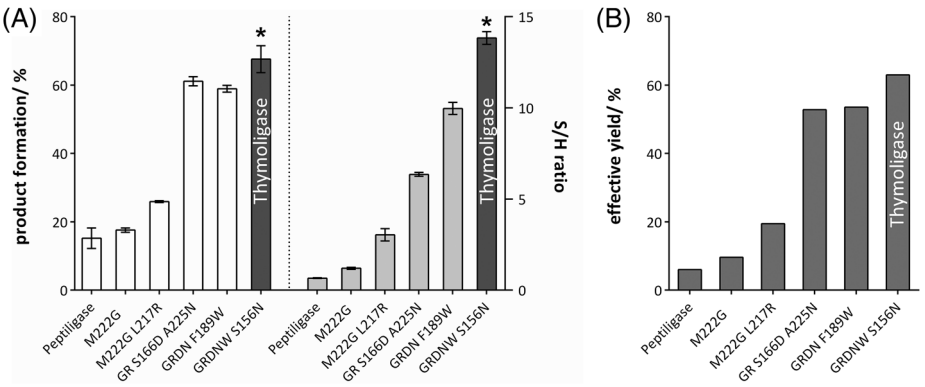

Fig. 4 Overall comparison of the evolutionary stages of the development from peptiligase to thymoligase. Results of the screening of several variants for the thymosin-α_1 [14 + 14]-mer coupling efficiency are shown. (A) Product formation (%) and S/H ratios after 60 min are shown. Screening conditions are identical to the ones shown in Fig. 3. Errors are depicted as the SEM (standard error of mean) and the arithmetic mean is shown. The best hit (thymoligase) is marked with a star (*). Due to the altered reaction conditions compared to those shown in Fig. 2A, deviating values for product formation (%) and S/H ratio were obtained for peptiligase, Ptl G, Ptl GR and Ptl GRDN. The screening conditions were identical to the ones shown in Fig. 3. (B) Effective yields after 60 min are shown. The effective yield represents a virtual measure of coupling efficiency. Effective yields are calculated by multiplying the amount of product formation after 60 min (%) with the S/H ratio (%).

crystallography (pdb code: 5OX2). This revealed structural conformity between the model of thymoligase used and its experimentally determined structure. The structural alignment between the homology model of thymoligase and its corresponding crystal structure has a root-mean square deviation (RMSD) of 0.4 Å over 266 aligned residues with 95.1% sequence identity. The general fold of subtilisin is preserved well in thymoligase and the mutations that are incorporated into the substrate binding clefts lead only to little structural change of the local topology, without disturbing the overall fold. Therefore, the assessment of our models docked with a partial substrate seemed to be suitable for a rational design approach.

Unexpectedly, in the crystal structure, a nonapeptide (VEEDHVAHA) derived from the prosequence of thymoligase (residues 68′–76′; prime symbols indicate the prosegment) was observed in the substrate-binding region and occupied sites S4–S2 but left position S1 empty (Fig. S1 and S3A†). The nonapeptide has several hydrogen bonds to main chain atoms of thymoligase, namely 76′N-O100, 75′O-127N, 75′N-127O, 74′O-102N, 74′N-102O, 72′O-104N, 72′Nδ1-131O, 71′Oδ1-104N, 71′Oδ1-105N, 71′Oδ2-Oγ105Ser and 71′Oδ2-Oε103Gln (Fig. S2†). The first two amino acids (V′68-E′69) of the peptide, visible in the electron density (Fig. S3B†), exhibit interactions with two symmetry-related thymoligase molecules and these two amino acids are found near the S2′ pocket of one of these molecules (^{16}Leu in the peptide model). The side chain of His75′ (P3) has a hydrogen bond to Oδ1 of Asn109 of a symmetry related molecule. Comparison with other subtilisin–propeptide complexes indicated that the main chain atoms of residues 71′–76′ (DHVAHA) of the nonapeptide overlay well with the propeptide observed in the crystal structure of a prosegment–subtilisin BPN′ complex (pdb code: 1SPB)[36] but deviate at residues 68′–70′ (VEE), while His75′ also has a different conformation. Moreover, the main chain atoms of the nonapeptide also overlap with the stabilized subtilisin prodomain in 3CNQ.[37] This prodomain extends across the (modified) active site of the S221A mutant by the addition of four residues at its C-terminus (from 68′ to 79′ VEEDKLYRALSA, in which H72′K, A74′Y, H75′R and Y77′L are mutated).

When the ^{6}D–^{18}E segment of thymosin-α_1 (bold in Ac-SDAAV**DTSSEITTKDLKE**KKEVVEEAEN-NH_2) was modeled into the active site of thymoligase, with ^{11}I–^{16}L in the P4–P2′ subsites, it appeared that residues P4–P2 of thymosin-α_1 (ITT) and of the propeptide (AHA) had the same position, but the peptide conformations may be different beyond this region (Fig. S3C†). The mutations S156N, at the S1 cleft rim, and S166D, at the bottom of the S1 site, create a hydrogen bond between the Nδ1 of N156 and the Oδ1 of D166 (2.9 Å). The walls of the S1 pocket are shaped by G118, G119 and the backbone atoms of L117 on one side, and by N146 on the other side. The Nε of ^{14}Lys would perfectly fit in this modified S1 pocket and would be capable of forming a salt bridge to the Oδ2 of D166, similar to the observed hydrogen bond between the Nε of ^{14}Lys and the Oδ2 of D166 in the model of peptiligase GRDN. However, an irregular, disordered structure of the substrate residue ^{14}Lys in the models of different peptiligase variants suggests that there is no clearly defined orientation of this residue.

Generally, the inspection of the thymoligase crystal structure can explain its improved performance in the synthesis of thymosin-α_1. Two important amino acids shaping the most discriminating nucleophile binding pocket S1′ for peptide ligation are M222 and L217.[13] Mutation M222G was expected to enhance the size of the pocket and thereby to widen the range of amino acids that is accepted. Indeed, the S1′ pocket is much widened in the crystal structure, while the φ/ψ angles of the residue M222G are not changed. Mutation A225N stabilizes the α-helix in which it is located with the formation of extra hydrogen bonds, also to the side chains of N123 and S125 and the main chain of 221O. As a result, the S1′ pocket has become more polar so that the carboxylate side chain of ^{15}Asp of the thymosin-α_1 acyl acceptor segment is better accommodated. Mutation L217R increases the size of the S1′ pocket even more by folding back the R217 side chain to the β-strand and forming a hydrogen bond with 216O. Unexpectedly, the hydrophobicity of the S1′ pocket is not changed by this substitution, and the Cδ2 of L217 overlaps with the Cδ of L217R. The important thymoligase F189W mutation in the S2′ pocket, which should accommodate ^{16}Leu, has no influence on the local backbone conformation, and the six-membered ring of the W189 side chain superimposes well on the wild type F189 side chain. However, the larger surface of the Trp side chain enlarges a platform that can contribute to hydrophobic contacts with the peptide ^{16}Leu side chain and therefore enhance the coupling efficiency.

In spite of the overall good agreement between the model used for designing the mutations and the crystal structure of thymoligase, there were some deviations. For example, the striking effect of the A225N mutation was originally suspected to be due to the binding of water between His67 and Asn225, but these are 1.6 Å more apart in the model compared to the crystal structure (4.8 Å). In addition, the conformation of Cys221 in the model is different from the conformation observed in the crystal structure and in 1GNV and 1SBN. In the model, the sulfur atom is directed towards M222G, while in the crystal structure it is directed between P1 and P1′, which more closely reflects an active conformation. In contrast, some active site backbone changes in the crystal structure are smaller than expected.

[14 + 14] segment ligation using thymoligase on a gram scale

The solid-phase synthesis of both [14]-mer segments was improved on a gram scale to 84% yield and 73% HPLC purity (net peptide content 64%) for the acyl donor Cam-ester segment, and 75% crude yield and 88% HPLC purity (net product content 90%) for the acyl acceptor segment, respectively (for the details of the synthesis see the Experimental section). After the discovery of thymoligase and the improved SPPS of the respective 14-mer segments on a larger scale, we successfully demonstrated the scalability of the [14 + 14] thymosin-α_1 segment condensation. Using thymoligase

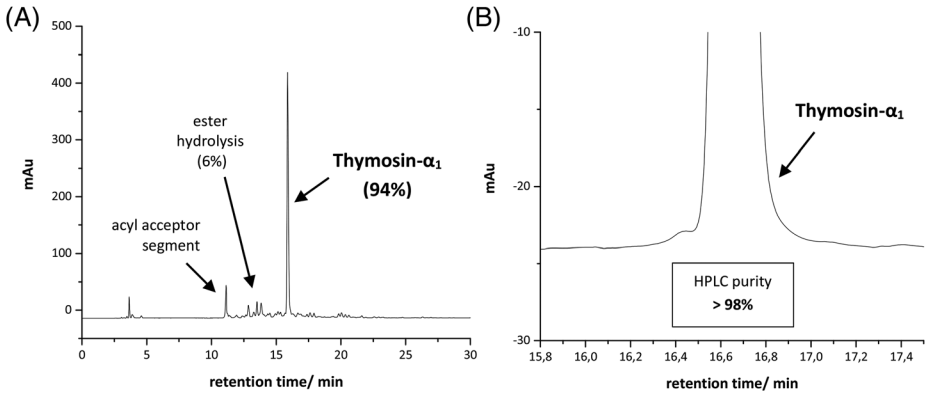

Fig. 5 (A) HPLC chromatogram (λ = 220 nm) of the crude reaction mixture of a [14 + 14]-mer thymosin-α_1 condensation on a gram scale using thymoligase. Product formation was 94% with only 6% of Cam-ester hydrolysis. CEPS was performed at room temperature (20 °C) in aqueous solution (1 M potassium phosphate, pH 8.3, 1 mg mL^{-1} TCEP; 1 g Ac-Thm(1–14)-OCam-Leu-OH with 1.2 eq. of the amine segment H-Thm(15–28)-OH were used. (B) Zoom in the HPLC spectrum (λ = 220 nm) of thymosin-α_1 after a single HPLC purification.

(0.0002 molar equivalents) under optimized reaction conditions (1 M phosphate, pH 8.3, 3.5 mM TCEP, room temperature), the crude acyl donor segment Ac-Thm(1–14)-OCam-Leu-OH was coupled with only 1.2 eq. of the crude acyl acceptor segment H-Thm(15–28)-OH on a gram scale. To the dissolved acyl acceptor segment (1.2 eq.), a total amount of 1 g crude Cam-ester segment was added over time (200 mg every 30 min), corresponding to a final crude substrate concentration of more than 250 g L^{-1}. The addition of TCEP to the reaction mixture was crucial, since the enzyme was significantly more active under reducing conditions (Fig. S18†). The quantitative conversion of the acyl donor segment after 4 hours of reaction time resulted in >94% product yield (Fig. 5A). Less than 6% of ester hydrolysis was observed (Fig. 5A), corresponding to an S/H ratio of more than 16. The rate determining step of the reaction appeared to be the dissolution of the Cam-ester segment. The dissolved part of the Cam-ester segment was immediately and predominantly converted to the thymosin-α_1 product, thus limiting the amount of ester hydrolysis. The crude HPLC purity of thymosin-α_1 in the reaction mixture could be increased from 62% to 78% by the precipitation of the product at pH 3.8 and subsequent washes with a buffer solution (100 mM ammonium acetate, pH 3.8, 0 °C). A single RP-HPLC purification of the crude reaction mixture resulted in over 98% HPLC purity (Fig. 5B). The net peptide content of the highly enantiopure product was determined to be 82.4% (Fig. S17†). A clearly improved separation of impurities from the product peak during HPLC purification was achieved compared to straight-through SPPS of the 28-mer and the overall yield of the CEPS approach was calculated to be 55%, which is two times more than the yields obtained using straight-through SPPS. In addition, using doped reversed phase (DRP) HPLC purification (ZeochemDRP 120 C5/10 μm column material, gradient: 5–8% acetonitrile in 40 min), we further reduced the solvent consumption during HPLC purification by more than 50% while retaining the product purity and overall yield.

Conclusion

Chemo-enzymatic peptide synthesis appears to be a viable and scalable strategy for the efficient and cost-optimized production of thymosin-α_1 using a [14 + 14]-mer ligation strategy on a gram scale (>94% coupling yield). During several generations of structure-inspired enzyme engineering, we discovered thymoligase, an enzyme that features a more than 5-fold higher catalytic efficiency and a more than 20-fold increased S/H ratio compared to its parent enzyme peptiligase. Thymoligase was specifically tailored for the thymosin-α_1 [14 + 14] coupling by introducing selected key mutations into the respective pockets, *i.e.* to accept positively and negatively charged amino acid residues in positions P1 and P1′. We expect thymoligase to be well applicable to many other ligations in which residues with similar characteristics (*e.g.* Arg and Glu) are present in the respective positions P1 and P1′. The quality of the homology models used for the design approach was examined by comparing with the 3D-structure obtained by X-ray crystallography. This indicated overall good agreement but local deviations are observed, especially in the binding of water molecules to the mutated side chains that influenced the synthetic performance. Using the optimized enzyme scaffold of thymoligase for the [14 + 14]-mer segment condensation, we were able to synthesize thymosin-α_1 in a significantly increased yield (55%), which is more than two-fold higher as compared to those typical for existing industrial processes. Due to an improved separation of impurities from the product peak compared to straight-through SPPS, the product was obtained in over 98% purity after only a single HPLC purification. Therefore, this process could lead to a very significant reduction of manufacturing costs. In addition, the CEPS strategy does not only provide a promising avenue for the synthesis of thymosin-α_1, but can also be used to produce several other linear (*e.g.* the incretin mimetic exenatide[13]) and cyclic[33,38] therapeutic peptides. Therefore, CEPS repre-

sents a powerful and broadly applicable tool for the large scale production of peptide therapeutics.

Experimental section

Enzyme engineering: computational approach

The models of peptiligase with the protease inhibitor eglin bound to the active site were generated based on a hybrid model, which was constructed with YASARA using the pdb files 1GNV[30] and 1SBN[31] as templates. Further mutations were incorporated using a YASARA script and a segment of thymosin-α_1 [7–19] modelled into the substrate binding region. The YASARA script applies the desired sidechain mutations and allows the surrounding residues to adapt to the mutations. After the new mutations were introduced into the three-dimensional structure of the protein, the new mutations were optimized by 6 repetitive cycles of energy optimization with stepwise dead-end elimination (DEE) optimization based on rotamers, followed by a local energy minimization in water. The volume that is energy optimized starts at 7 Å from the mutated residues and increases with 1 Å every cycle, finally resulting in an energy optimization of the entire enzyme scaffold. The numbering of mutations is based on subtilisin BPN′.[39]

Construction of peptiligase variants

Peptiligase variants were prepared by using a Quikchange site-directed mutagenesis kit using the pBE-S-peptiligase vector as the template plasmid.[12] The *E. coli–B. subtilis* shuttle vector pBE-S (Takara Bio Inc.) included the *aprE* promoter sequence, the peptiligase secretion signal peptide and the sequence followed by a C-terminal hexahistidine tag and a terminator sequence. DpnI-digested and purified plasmids were transformed to competent *E. coli* TOP10 and transformants were plated on LB-agar plates containing 100 μg mL^{-1} ampicillin. The mutant genes were confirmed by DNA sequencing.

Expression and purification of peptiligase variants

For the production of the enzyme variants, the respective mutant vector was transformed into *B. subtilis* GX4935 (*trpC2 metB10 lys-3 ΔnprE ΔaprE*), which is a strain deficient in extracellular neutral and serine proteases and was a kind gift from Prof. P.N. Bryan (University of Maryland, USA).[40] After overnight incubation on LB-agar plates, colonies were picked and grown overnight in 5 mL LB with kanamycin (10 μg mL^{-1}) at 37 °C in a shaking incubator. 0.6 mL of the culture were added to 30 mL Terrific Broth medium supplemented with antibiotic (kanamycin 10 μg mL^{-1}) and amino acids (100 mg L^{-1} Trp, 100 mg L^{-1} Met and 100 mg L^{-1} Lys). The cells were grown for 48 h at 37 °C in a shaking incubator, before being harvested by centrifugation (4 °C). The supernatant was concentrated by ultrafiltration (Amicon-centrifugal unit, 10 kDa MW cut-off) in two centrifugation steps. The concentrated medium was then exchanged to buffer A (25 mM tricine, 0.5 M NaCl, pH 7.5). Talon resin (Clontech) was used for gravity-flow His-tag purification. After washing the resin with MilliQ water (5 CV) and equilibration with buffer A (10 CV), the crude enzyme was loaded on the column and washed with 10 CV buffer A. The enzyme was eluted with 3 CV buffer B (25 mM tricine, pH 7.5, 0.5 M NaCl, 200 mM imidazole). The eluate was concentrated with a Amicon-centrifugal unit (10 kDa MW cut-off) by centrifugation and the buffer was exchanged to the storage buffer (25 mM tricine, pH 7.5). The protein concentration was determined using UV/VIS spectrophotometry (λ = 280 nm) and the purity was assessed *via* SDS-PAGE. The purity was estimated to be >80% (Fig. S4–S6†). The purified enzyme was flash-frozen in liquid nitrogen and stored at −80 °C until further use.

Testing of peptiligase variants

The ligation reactions were typically performed at 20 °C in a 96-well plate. Two different stock solutions were prepared, (i) crude Ac-Thm(1–14)-OCam-Leu-OH (7.15 mM) and crude H-Thm(15–28)-OH (8.55 mM) in 1 M potassium phosphate buffer (pH 8.0, 3.5 mM TCEP) and (ii) enzyme solution in MilliQ water (0.2 mg mL^{-1} of each peptiligase variant). The reactions were started by adding 190 μL of solution (i) to 10 μL of solution (ii). Aliquots of 8 μL were quenched in 1 mL acetonitrile (ACN)/H_2O (1 : 2 (v/v); 0.2% methanesulfonic acid (MSA) (v/v)) after 2.5, 5, 7.5, 10, 15, 30 and 60 min and analyzed by RP-HPLC (λ = 220 nm) using a ReProSil-Pur C18 5 μm, 4.6 × 250 mm (Dr Maisch, Ammerbuch, Germany) column. As a mobile phase a binary mixture of A (water + 0.05% MSA) and B (ACN + 0.05% MSA) was used by default. Samples were separated using a gradient of 12 to 30 vol% B in A in 21 min at a flow of 1 mL min^{-1} and 40 °C column temperature. All measurements were performed in triplicate and the arithmetic mean was calculated. Errors are depicted as the SEM (standard error of mean). The product formation was calculated by automatically integrating the HPLC peaks of the Cam-ester, its hydrolysis product and the corresponding coupling product. The synthesis over hydrolysis ratio (S/H ratio) was calculated after every time point by dividing the amount of the product by the amount of the hydrolyzed Cam-ester. Because some spontaneous hydrolysis occurs while dissolving the substrates before the reaction start, values were corrected for initial chemical background hydrolysis by subtracting the percentage of the hydrolysis of blank Ac-Thm(1–14)-OCam-Leu-OH (without enzyme) at t = 2.5 min from each value measured in time. Effective yields are given as a virtual measure of coupling efficiency. They were calculated by multiplying the amount of product formation after 60 min (%) with the S/H ratio (%).

After screening the first variants (Fig. 2), the substrate and enzyme concentration was halved and the pH was lowered to pH 8.0 for the second and third screening (Fig. 3 and 4) in order to clearly highlight the differences between peptiligase variants. The differences between the enzyme variants are easier to visualize using these slightly adapted conditions: 1 M phosphate, pH 8.3, 3.5 mM TCEP, room temperature, 0.7 μM of enzyme, crude Ac-Thm(1–14)-OCam-Leu-OH (14.3 mM) and crude H-Thm(15–28)-OH (17.1 mM).

Synthesis of Fmoc-Lys(Boc)-*O*-glycolic acid (according to Nuijens *et al.*[41])

2-CTC resin (50 g, 55 mmol) was swollen in dichloromethane (DCM) and washed with dimethylformamide (DMF). The resin was activated with a 15% (v/v) solution of $SOCl_2$ in DMF by stirring overnight. The resin was washed with DMF and DCM. Glycolic acid (0.11 mol, 2 eq.) was dissolved in DCM and DIPEA (0.22 mol, 4 eq.) was added. The resulting solution was added to the resin and the mixture was stirred for 60 min, before the resin was washed with DCM, and unreacted chloride was capped by adding a mixture of DCM/methanol/DIPEA (80/15/5 (v/v/v)). The resin was washed with DCM and DMF, and the ester bond was formed by adding a solution of Fmoc-L-Lys-OH (0.22 mol, 4 eq.), DMAP (22 mmol) and DIC (0.22 mol, 4 eq.). The mixture was stirred for 60 min, and the resin was washed with DMF and DCM. Cleavage was performed with 5% TFA (v/v) in DCM (3 × 15 min). The filtrates were collected and washed with demineralized water and brine. The organic phase was collected and dried on sodium sulfate. After washing the solid with DCM, the combined filtrates were concentrated *in vacuo* to yield a white powder (26 g, 49.4 mmol, 90% yield). The final product was purified *via* preparative HPLC.

Synthesis of Ac-Thm(1–14)-OCam-Leu-OH

7.2 gram of Fmoc-Leu Wang resin (loading of 0.7 mmol g^{-1}) was washed with dichloromethane (DCM) and DMF. Fmoc deprotection was performed using piperidine/DMF (1/4 (v/v)). After washing with DMF, DCM and DMF, Fmoc-Lys(Boc)-*O*-glycolic acid (10 mmol) was coupled with the resin using HBTU (4 eq.) and OxymaPure (4 eq.) in DMF (45 min). After washing with DMF, DCM and DMF, Fmoc deprotection was performed (piperidine/DMF) (1/4 (v/v)). The following Fmoc protected amino acids were coupled using 4 eq. Fmoc-AA-OH, 4 eq. HBTU, 4 eq. OxymaPure and 8 equiv. diisopropylethylamine (DIPEA) in DMF for 45 min. After washing with DMF, DCM and DMF, cycles of washing, deprotection and coupling were performed repeatedly to elongate the peptide. In order to overcome severe diketopiperazine formation and to prevent β-sheet formation of the aggregation prone sequence ^{11}Ile–^{12}Thr–^{13}Thr–^{14}Lys,[26] two pseudoproline building blocks, *i.e.* Fmoc-L-Asp(*t*Bu)-L-Thr[ψ(Me,Me)Pro]-OH and Fmoc-L-Thr(*t*Bu)-L-Thr[ψ(Me,Me)Pro]-OH, were introduced at positions ^{6}Asp–^{7}Thr and ^{12}Thr–^{13}Thr, respectively. In these cases, the coupling time was extended to 90 min. Finally, N-terminal acetylation was performed using a mixture of DMF/OxymaPure/DIPEA/Ac_2O (450 mL/1.03 g/9.82 mL/21.3 mL) for 30 min. Cleavage from the resin and sidechain deprotection was performed using a mixture of trifluoroacetic acid (TFA), triisopropylsilane (TIS) and water (95/2.5/2.5, v/v/v) for 120 min. The crude peptide was precipitated using methyl *tert*-butyl ether (MTBE)/*n*-heptane, followed by drying under reduced pressure at 35 °C overnight. The lyophilization of the peptide segment was omitted in order to reduce the amount of aspartimide formation.

Synthesis of H-Thm(15–28)-OH

18.5 g of Fmoc-Asn(Trt) Wang resin (loading of 0.27 mmol g^{-1}) was washed with DCM and DMF. Fmoc deprotection was performed using piperidine/DMF (1/4 (v/v)). After washing with DMF, repetitive cycles using standard SPPS protocols (4 eq. Fmoc-AA-OH, 4 eq. HBTU, 4 eq. OxymaPure, 8 eq. DIPEA, 45 min) were followed to elongate the peptide, with couplings of amino acids 15 to 21 performed for 90 min. In general, a low resin loading and double couplings in a sequence of mostly charged amino acids significantly increased the overall purity. Cleavage from the resin and sidechain deprotection was performed using a mixture of TFA/TIS/phenol (95/2.5/2.5, v/v/v) for 120 min. The crude peptide was precipitated using MTBE/*n*-heptane (1/1 (v/v)), followed by drying under reduced pressure at 35 °C overnight. The lyophilization of the peptide segment was omitted in order to reduce the amount of deamidation of the C-terminal Asn.

Determination of the net product content

For the assessment of the net product content of peptide samples, the corresponding peptide was purified to an HPLC purity of >98% *via* RP-HPLC. A dilution series of suitable concentrations (H-Thm(15–28)-OH: 0.2–2.0 mg mL^{-1}; Ac-Thm(1–14)-OCam-Leu-OH: 0.0034–0.43 mg mL^{-1}) was prepared and analyzed with analytical HPLC (λ = 220 nm) using a ReProSil-Pur C18 5 μm, 4.6 × 250 mm (Dr Maisch, Ammerbuch, Germany) column. As a mobile phase, a binary mixture of A (water + 0.05% MSA) and B (ACN + 0.05% MSA) was used by default. The elution conditions were chosen individually for each peptide. If not mentioned explicitly, the curves refer to an HPLC injection volume of 25 μL. The linear regression of data points was performed using GraphPad Prism 6.

[14 + 14]-mer CEPS of thymosin-α_1

The crude amine nucleophile segment H-Thm(15–28)-OH (1.1 g, 0.47 mmol) was dissolved in 5 mL potassium phosphate buffer (1 M, pH 8.3, 3.5 mM TCEP) and 2 mg of thymoligase (0.0002 molar equivalents) were added from a stock solution (c = 26 mg mL^{-1}). The crude Cam-ester segment Ac-Thm(1–14)-OCam-Leu-OH (1 g, 0.37 mmol) was added over time (200 mg every 30 min). The pH was kept constant at pH 8.3 (titration with acid/base), resulting in a final reaction volume of 7.5 mL. The mixture was stirred at room temperature (20 °C) for a total of 4 hours. The reaction progress was monitored by HPLC-MS (λ = 220 nm). The crude reaction mixture was diluted with ACN/H_2O (3/1 (v/v)) to 100 mL and 50 mL were directly purified by RP-HPLC and freeze-dried. Thymosin-α_1 was obtained in an overall yield of 55%. For purification, a Luna Prep C18 column (10 μm, 200 × 51 mm, Phenomenex, Torrance, CA, USA) with a gradient of 16 to 28% ACN/H_2O (0.05% TFA) in 42 min and a flow rate of 45 mL min^{-1} was used.

Conflicts of interest

There are no conflicts to declare.

Acknowledgements

The authors wish to thank Dr E. R. Lax for useful discussions and providing corrections to this manuscript, Dr A. Burkhardt for the assistance in using the beamline and Dr E. R. Reddem for X-ray data collection.

References

1 K. Fosgerau and T. Hoffmann, *Drug Discovery Today*, 2015, **20**, 122–128.
2 J. L. Lau and M. K. Dunn, *Bioorg. Med. Chem.*, DOI: 10.1016/j.bmc.2017.06.052.
3 E. R. Lax, *Chem. Today*, 2016, **34**, 22–27.
4 R. B. Merrifield, *J. Am. Chem. Soc.*, 1963, **85**, 2149–2154.
5 J. M. Antos, M. C. Truttmann and H. L. Ploegh, *Curr. Opin. Struct. Biol.*, 2016, **38**, 111–118.
6 G. K. T. Nguyen, S. Wang, Y. Qiu, X. Hemu, Y. Lian and J. P. Tam, *Nat. Chem. Biol.*, 2014, **10**, 732–738.
7 G. K. T. Nguyen, Y. Qiu, Y. Cao, X. Hemu, C. Liu and J. P. Tam, *Nat. Protoc.*, 2016, **11**, 1977–1988.
8 C. Meyer, S. Liebscher and F. Bordusa, *Bioconjugate Chem.*, 2016, **27**, 47–53.
9 S. Liebscher, P. Kornberger, G. Fink, E. M. Trost-Gross, E. Höss, A. Skerra and F. Bordusa, *ChemBioChem*, 2014, **15**, 1096–1100.
10 L. Abrahmsen, J. Tom, J. Burnier, K. A. Butcher, A. Kossiakoff and J. A. Wells, *Biochemistry*, 1991, **30**, 4151–4159.
11 S. H. Henager, N. Chu, Z. Chen, D. Bolduc, D. R. Dempsey, Y. Hwang, J. Wells and P. A. Cole, *Nat. Methods*, 2016, **13**, 925–927.
12 A. Toplak, T. Nuijens, P. J. L. M. Quaedflieg, B. Wu and D. B. Janssen, *Adv. Synth. Catal.*, 2016, **358**, 2140–2147.
13 T. Nuijens, A. Toplak, P. J. L. M. Quaedflieg, J. Drenth, B. Wu and D. B. Janssen, *Adv. Synth. Catal.*, 2016, **358**, 4041–4048.
14 M. Schmidt, A. Toplak, P. J. L. M. Quaedflieg and T. Nuijens, *Curr. Opin. Chem. Biol.*, 2017, **38**, 1–7.
15 J. Li, C. H. Liu and F. S. Wang, *Peptides*, 2010, **31**, 2151–2158.
16 C. Tuthill, I. Rios and R. McBeath, *Ann. N. Y. Acad. Sci.*, 2010, **1194**, 130–135.
17 C. Tuthill, *Ann. N. Y. Acad. Sci.*, 2007, **1112**, 351–356.
18 B. C. Birr and U. Stollenwerkt, *Angew. Chem., Int. Ed. Engl.*, 1979, **18**, 394–395.
19 J. Swistok, M. Roszkowski, M. Ahmad, D. Confalone, J. W. Scott, D. Parker, J. Meienhofer, A. Trzeciak and D. Gillessen, *Int. J. Pept. Protein Res.*, 1985, **26**, 130–148.
20 S. S. Wang, R. Makofske, A. Bach and R. B. Merrifield, *Int. J. Pept. Protein Res.*, 1980, **15**, 1–4.
21 S. S. Wang, I. D. Kulesha and D. P. Winter, *J. Am. Chem. Soc.*, 1979, **101**, 253–254.
22 T. W. Wong and R. B. Merrifield, *Biochemistry*, 1980, **19**, 3233–3238.
23 M. Mokotoff and A. Patchornik, *Int. J. Pept. Protein Res.*, 1983, **21**, 145–154.
24 H. Echner, *Liebigs Ann. Chem.*, 1988, **1988**, 1095–1097.
25 Y. García-Ramos, M. Giraud, J. Tulla-Puche and F. Albericio, *Biopolym. Pept. Sci.*, 2009, **92**, 565–572.
26 C. Toniolo, G. M. Bonora, E. P. Heimer and A. M. Felix, *Int. J. Pept. Protein Res.*, 1987, **30**, 232–239.
27 Y. Ren, X. Yao, H. Dai, S. Li, H. Fang, H. Chen and C. Zhou, *Microb. Cell Fact.*, 2011, **10**, 26.
28 R. S. Esipov, V. N. Stepanenko, K. A. Beyrakhova, T. I. Muravjeva and A. I. Miroshnikov, *Biotechnol. Appl. Biochem.*, 2010, **56**, 17–25.
29 C. E. Stauffer and D. Etson, *J. Biol. Chem.*, 1969, **244**, 5333–5338.
30 O. Almog, D. T. Gallagher, J. E. Ladner, S. Strausberg, P. Alexander, P. Bryan and G. L. Gilliland, *J. Biol. Chem.*, 2002, **277**, 27553–27558.
31 D. W. Heinz, J. P. Priestle, J. Rahuel, K. S. Wilson and M. G. Grütter, *J. Mol. Biol.*, 1991, **217**, 353–371.
32 J. A. Wells, D. B. Powers, R. R. Bott, T. P. Graycar and D. A. Estell, *Proc. Natl. Acad. Sci. U. S. A.*, 1987, **84**, 1219–1223.
33 M. Schmidt, A. Toplak, P. J. L. M. Quaedflieg, H. Ippel, J. J. Gaston, T. M. Hackeng, J. H. Van Maarseveen and T. Nuijens, *Adv. Synth. Catal.*, 2017, **359**, 2050–2055.
34 T. Nuijens, A. Toplak, M. B. A. C. van de Meulenreek, M. Schmidt, M. Goldbach, P. J. L. M. Quaedflieg and D. B. Janssen, *Chem. Today*, 2016, **34**, 16–19.
35 P. Bryan, M. W. Pantoliano, S. G. Quill, H. Y. Hsiao and T. Poulos, *Proc. Natl. Acad. Sci. U. S. A.*, 1986, **83**, 3743–3745.
36 T. Gallagher, G. Gilliland, L. Wang and P. Bryan, *Structure*, 1995, **3**, 907–914.
37 B. Ruan, V. London, K. E. Fisher, D. T. Gallagher and P. N. Bryan, *Biochemistry*, 2008, **47**, 6628–6636.
38 M. Schmidt, A. Toplak, P. J. L. M. Quaedflieg, J. H. van Maarseveen and T. Nuijens, *Drug Discovery Today: Technol.*, 2017, **26**, 11–16.
39 O. Almog, T. Gallagher, M. Tordova, J. Hoskins, P. Bryan and G. L. Gilliland, *Proteins*, 1998, **31**, 21–32.
40 S. R. Fahnestock and K. E. Fisher, *Appl. Environ. Microbiol.*, 1987, **53**, 379–384.
41 T. Nuijens, A. Toplak, M. B. A. C. Van De Meulenreek, M. Schmidt, M. Goldbach and P. J. L. M. Quaedflieg, *Tetrahedron Lett.*, 2016, **57**, 3635–3638.

